Journal of Medicinal Chemistry

pubs.acs.org/jmc

Article

Bioisosteric Discovery of NPA101.3, a Second-Generation RET/VEGFR2 Inhibitor Optimized for Single-Agent Polypharmacology

Marialuisa Moccia, Brendan Frett, Lingtian Zhang, Naga Rajiv Lakkaniga, David C. Briggs, Rakhee Chauhan, Annalisa Brescia, Giorgia Federico, Wei Yan, Massimo Santoro, Neil Q. McDonald, Hong-yu Li,* and Francesca Carlomagno*

Cite This: J. Med. Chem. 2020, 63, 4506−4516

Read Online

ACCESS | Metrics & More | Article Recommendations | Supporting Information

ABSTRACT: RET receptor tyrosine kinase is a driver oncogene in human cancer. We recently identified the clinical drug candidate Pz-1, which targets RET and VEGFR2. A key *in vivo* metabolite of Pz-1 is its less active demethylated pyrazole analogue. Using bioisosteric substitution methods, here, we report the identification of NPA101.3, lacking the structural liability for demethylation. NPA101.3 showed a selective inhibitory profile and an inhibitory concentration 50 (IC_{50}) of <0.003 μM for both RET and VEGFR2. NPA101.3 inhibited phosphorylation of all tested RET oncoproteins as well as VEGFR2 and proliferation of cells transformed by RET. Oral administration of NPA101.3 (10 mg/kg/day) completely prevented formation of tumors induced by RET/C634Y-transformed cells, while it weakened, but did not abrogate, formation of tumors induced by a control oncogene (HRAS/G12V). The balanced synchronous inhibition of both RET and VEGFR2, as well the resistance to demethylation, renders NPA101.3 a potential clinical candidate for RET-driven cancers.

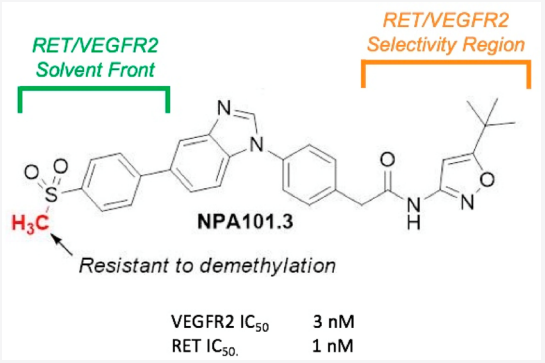

INTRODUCTION

RET (rearranged during transfection) is the receptor tyrosine kinase (RTK) for neurotrophic factors of the GDNF (glial cell line-derived neurotrophic factor) family.[1] In several human cancers, RET rearrangements lead to the formation of chimeric oncoproteins, containing the RET tyrosine kinase (TK) domain fused to the N-terminal region of heterologous proteins. These include papillary thyroid carcinoma (PTC),[2] medullary thyroid carcinoma (MTC),[3] lung adenocarcinoma,[4−6] chronic myeloproliferative disorders,[7,8] Spitz melanoma,[9] and colon,[10,11] breast,[12] and salivary duct[13] carcinomas. CCDC6 (coiled-coil domain containing 6)-RET rearrangement has also been found in EGFR (epidermal growth factor receptor) mutant lung adenocarcinoma patients who had progressed upon EGFR TKI treatment.[14] In addition, various types of germline point mutations activating the RET kinase are the causative event of hereditary MTC, in the frame of multiple endocrine neoplasia type 2 (MEN2A and MEN2B) syndromes. Somatic RET mutations, mostly RET/M918T, are commonly associated (∼50% of cases) to sporadic MTC.[1,15] Finally, RET is overexpressed in several malignancies, including breast[16,17] and pancreatic[18,19] carcinoma.

RET targeting with tyrosine kinase inhibitors (TKIs) has emerged as a promising molecular approach for the treatment of cancer.[20,21] Two TKIs, Vandetanib and Cabozantinib, were found to exhibit VEGFR2 (vascular endothelial growth factor receptor 2) and RET activity.[22,23] These two drugs have been approved to treat MTC because of their capability to prolong progression-free survival.[24,25] In addition, Sorafenib and Lenvatinib, two multikinase inhibitors with activity against RET, have been approved for the treatment of radioiodine-refractory differentiated thyroid cancer.[26,27] Novel TKIs, BLU-667, LOXO-292, and RXDX-105, have recently demonstrated promising clinical activity in RET-driven cancers.[28−30]

Toxicity, due to on- or off-targets effects, and resistance formation may limit the efficacy of TKIs in clinical practice. We sought to set up a fragment-based chemical screen to identify novel RET inhibitors. This approach led to the clinical candidate Pz-1, a type 2 TKI directed against RET and VEGFR2.[31]

In vivo stability is a critical factor that directly determines efficacy.[32] Through completion of investigative new drug (IND) studies, a demethylated less active metabolite of Pz-1 was identified. Here, by applying bioisosteric substitution of the Pz-1 site susceptible to demethylation, we report the

Received: August 14, 2019
Published: April 16, 2020

https://dx.doi.org/10.1021/acs.jmedchem.9b01336
J. Med. Chem. 2020, 63, 4506−4516

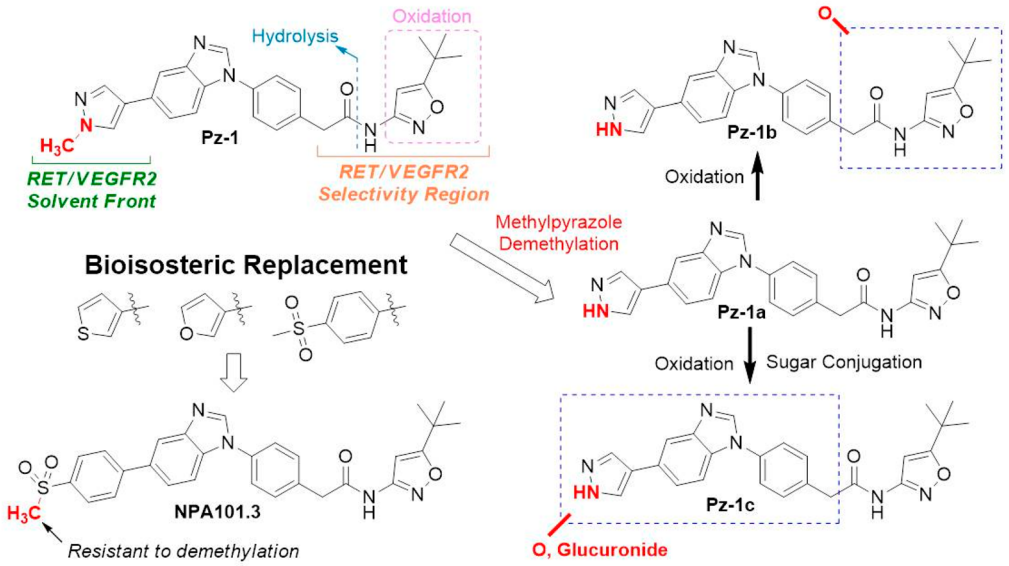

Figure 1. Metabolism of Pz-1 and bioisosteric replacement methods. Pz-1 is hydrolyzed, oxidized, or demethylated via phase 1 metabolic systems. Hydrolysis and oxidation occur in the selectivity region for binding to RET and VEGFR2, while demethylation occurs at the solvent front for both kinases. Bioisosteric replacement at the solvent front was performed by replacing methylpyrazole with (methylsulfonyl)benzene, generating NPA101.3. VEGFR2 DFG-out crystal structure (PDB entry 2OH4).

identification of NPA101.3 as a novel clinical TKI candidate and its characterization through *in vitro* and *in vivo* assays.

RESULTS

Discovery of NPA101.3. During IND studies of Pz-1, a series of *in vivo* metabolites were identified; via phase 1 metabolic systems, Pz-1 is oxidized, hydrolyzed, or demethylated, generating a less active derivative (Figure 1 and data not shown). Hydrolysis and initial oxidation occur in the selectivity region, which is the region of Pz-1 that enters the allosteric pocket of both RET and VEGFR2. Any modification to slow metabolism in this region can alter selectivity and inhibitory profiles and, therefore, is likely to alter the optimized RET/VEGFR2 inhibitory profile. Another major, metabolic pathway of Pz-1 is initiated via the phase 1 demethylation of methylpyrazole to generate Pz-1a. In turn, Pz-1a is further biotransformed via oxidation (to Pz-1b) or oxidation and sugar conjugation through phase 2 systems (to Pz-1c). Interestingly, the methylpyrazole substituent of Pz-1 is oriented toward the solvent and is not expected to contribute significantly to selectivity profiles[31,32] (Figure 1).

Bioisosteric replacement of the methylpyrazole of Pz-1 was investigated to generate an alternative clinical candidate with a similar polypharmacological profile but resistance to demethylation. In both RET and VEGFR2, the methylpyrazole binds to solvent-exposed regions, which can accommodate a variety of substituents. SAR (structure−activity relationship) studies have shown that replacement of methylpyrazole with various five-membered ring systems decreases inhibitory activity.[31] Therefore, substitution with polar, electron-deficient (methylsulfonyl)benzene was investigated. The methylsulfonyl group occupies the same chemical space as the methyl pyrazole and has the same hydrogen binding pattern at the computer modeling (data not shown); therefore, it is expected not to affect the pharmacological activity of the drug as compared to methylpyrazole. Importantly, analogues containing (methylsulfonyl)benzene do not carry the structural liability of demethylation. Therefore, the (methylsulfonyl)benzene was chosen as an appropriate bioisosteric replacement for methylpyrazole, to obtain the novel compound designated NPA101.3 (Figure 1). The chemical synthesis of NPA101.3 is described in the Supporting Information.

Computational Modeling of NPA101.3. NPA101.3 was modeled in the RET kinase DFG [aspartic acid (D892), phenylalanine (F893), glycine (G894)]-out computational model as previously described (Figure 2).[31] The model suggested that NPA101.3 binds to RET kinase in its inactive (DFG-out) conformation, as it is characteristic of type 2 TKIs.[33] The benzimidazole moiety acts as the "warhead", making a key hydrogen bond with A807 at the RET ATP binding site (hinge region). The benzimidazole also forms two $\pi-\pi$ stacking interactions with Y806. The *p*-sulfone substituent displays an orientation toward the solvent and engages K728 through a cation$-\pi$ interaction. The amide region interacts with D892 from the DFG motif through a hydrogen bond. This interaction opens a novel lipophilic pocket, which is effectively filled by *tert*-butyl isoxazole. The modeling predicted NPA101.3 to bind RET with high affinity and with a projected ΔG of −11.9 kcal/mol. Moreover, the model indicated that binding of NPA101.3 was not influenced by substitutions of V804, which is the gatekeeper residue whose replacement with a methionine or a leucine confers resistance to Vandetanib, Cabozantinib, and several other inhibitors (Figure 2 and Table S1).[29,34−36] NPA101.3 was also predicted to bind VEGFR2 with comparable high affinity (Figure 2). Indeed, similar to Pz-1, the free rotation of the methylene linker permits a tailored orientation of the isoxazole in the allosteric pocket of both RET and VEGFR2, enabling balanced inhibition of both kinases.[31]

To further address the type of binding, we docked sorafenib in the RET model and compared docking poses between the RET−sorafenib and VEGFR2−sorafenib (PDB entry 3WZE) complexes. The poses were nearly identical, further suggesting NPA101.3 is a type 2 inhibitor (Figure S1).

Kinase Inhibitory Activity of NPA101.3. We tested the ability of NPA101.3 to inhibit RET, the RET/V804M mutant,

https://dx.doi.org/10.1021/acs.jmedchem.9b01336
J. Med. Chem. 2020, 63, 4506−4516

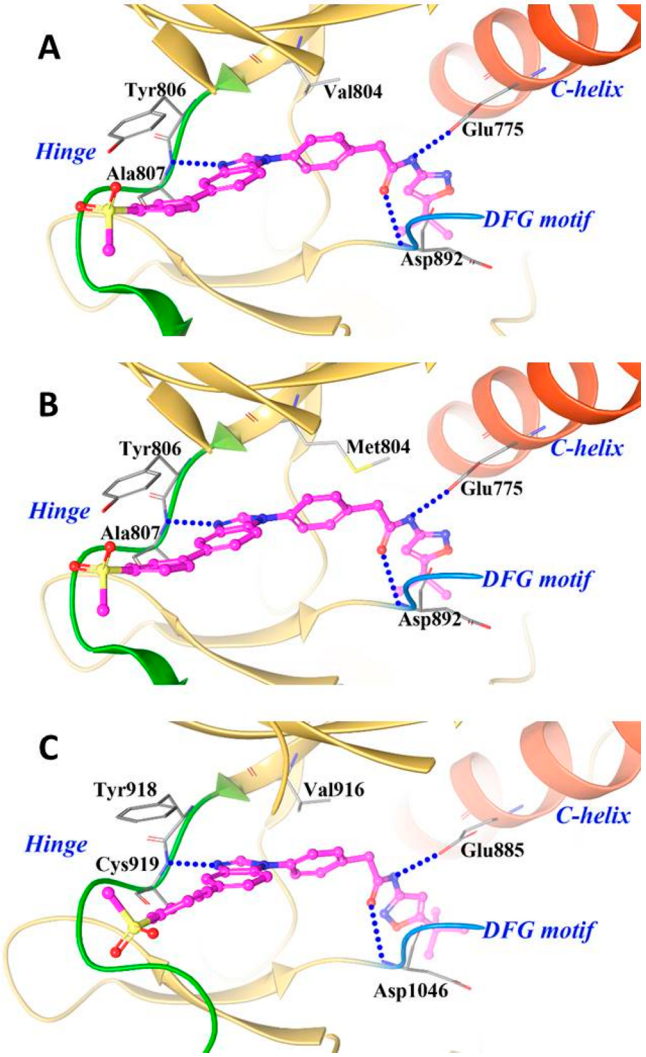

Figure 2. Computational modeling of NPA101.3. (A) NPA101.3 computationally modeled in a RET DFG-out homology model. The model shows the hydrogen bond at the ATP binding site with A807, a hydrogen bond network at the DFG motif, and interaction with Y806 via $\pi-\pi$ stacking. The model also shows that *p*-sulfone of NPA101.3 is solvent-exposed. Hydrogen bonds are shown with blue dotted lines. (B) NPA101.3 computationally modeled in a RET/V804M DFG-out homology model. NPA101.3 can accommodate bulky mutations at the gatekeeper residue. (C) NPA101.3 computationally modeled in the VEGFR2 kinase. The binding mode is nearly identical to the binding mode in RET, with the exception of the isoxazole orientation in the allosteric pocket. Flexibility at the methylene linker is predicted to permit the balanced affinity of NPA101.3 for RET and VEGFR2.

and VEGFR2 in an *in vitro* kinase assay. To determine if NPA101.3 tightly bound the kinase, we used a high concentration of ATP (190 μM). Such a high concentration is orders of magnitude greater than the K_m for either RET or VEGFR2 and reflects the high intracellular concentration of ATP (1−10 mM). NPA101.3 exhibited an inhibitory concentration 50 (IC_{50}) of 0.001 μM for RET, 0.008 μM for RET/V804M, and 0.003 μM for VEGFR2. Thus, NPA101.3 represents a novel RET/VEGFR2 dual inhibitor with a pharmacological profile similar to that of Pz-1.

To further investigate the binding of NPA101.3 to RET, a thermal shift assay was performed to monitor the protein melting temperature. This assay determines the drug-induced increase in the melting temperature (ΔT_m) of the isolated RET kinase domain, which reflects the stability of the kinase−ligand complex[37,38] and correlates with the inhibitor IC_{50}.[39] Addition of NPA101.3 increased the thermal stability of active and phosphorylated RET by a dramatic ΔT_m of 16 ± 1.1 °C, over a time course of 240 min (Figure 3C; a representative experiment is reported in Figure 3A). This was consistent with values seen for type 2 inhibitors, such as Sorafenib, stabilizing a DFG-out inactive conformer.[40] We observed the same magnitude of thermal shift by NPA101.3 for the wild type and V804M mutant (Figure 3B), confirming that the compound is insensitive to gatekeeper mutation. In contrast, a substantially smaller ΔT_m shift of 6.1 ± 3.3 °C was observed with the type 1 compound PP1 (Figure 3C), consistent with our previously published data.[38] As expected, the type 1 inhibitor PP1 was sensitive to gatekeeper mutation (Figure 3C). We conclude that NPA101.3 binds tightly to both wild type and V804M RET kinase domains in a type 2 binding mode.

In addition, NPA101.3, at a concentration of 100 nM, was subjected to a kinome scan against a 96-kinase panel representing major kinome clusters (Table S2). The compound featured good selectivity, displaying strong binding activity (>90% bound) for only seven additional kinases [CSF1R (colony stimulating factor 1 receptor), FRK (fyn-related Src family tyrosine kinase), HCK (HCK proto-oncogene, Src family tyrosine kinase), LYN (lyn proto-oncogene, Src family tyrosine kinase), MKNK2 (MAPK-interacting serine/threonine kinase 2), TRKA (neurotrophic receptor tyrosine kinase 1), and TRKC (neurotrophic receptor tyrosine kinase 3)] and weak binding (>10−35% bound) for six other kinases (Table S2 and Figure S2). It is important to note that the measurement of binding affinity, which is based on control ligand displacement (K_d), is more sensitive than the *in vitro* kinase assay. Among the seven kinases with >90% binding, TRKA and CSF1R were selected for an *in vitro* kinase assay. NPA101.3 was active against TRKA and CSF1R with IC_{50} values of 32 and 46 nM, respectively (Figure S3). Finally, we verified the ability of NPA101.3 to interfere with hERG (potassium voltage-gated channel subfamily H member 2) conductibility via a patch-clamp assay. As shown in Table S4, the IC_{50} dose of NPA101.3 for hERG was 7.57 μM (while it was 0.027 μM in the case of the positive control E-4031), thereby >7000-fold higher than that for RET (1 nM) (Table S3).

NPA101.3-Mediated Inhibition of RET and VEGFR2 Phosphorylation and Signaling. Fibroblasts transfected with RET/C634R were treated with increasing doses of NPA101.3, ranging from 0.1 to 10.0 nM. RET autophosphorylation was assessed by Western blotting using two different antibodies that can recognize phosphorylated Y905, located in the RET kinase activation loop, or Y1062, a multidocking site involved in RET downstream signaling.[41] As shown in Figure 4A, RET phosphorylation started to be inhibited at 0.3 nM and was almost completely blocked at 3.0 nM. NPA101.3 also inhibited other MTC-associated RET oncogenic point mutants, including RET/M918T, RET/A883F, and RET/V804L/M (Figure 4B). Rearranged RET oncoproteins (CCDC6-RET, NCOA4-RET, and FGFR1OP-RET) were highly sensitive to NPA101.3 inhibition, as well (Figure 4C). Finally, 1.0 nM NPA101.3 reduced the level of ligand-induced VEGFR2 autophosphorylation; inhibition was virtually total at

https://dx.doi.org/10.1021/acs.jmedchem.9b01336
J. Med. Chem. 2020, 63, 4506−4516

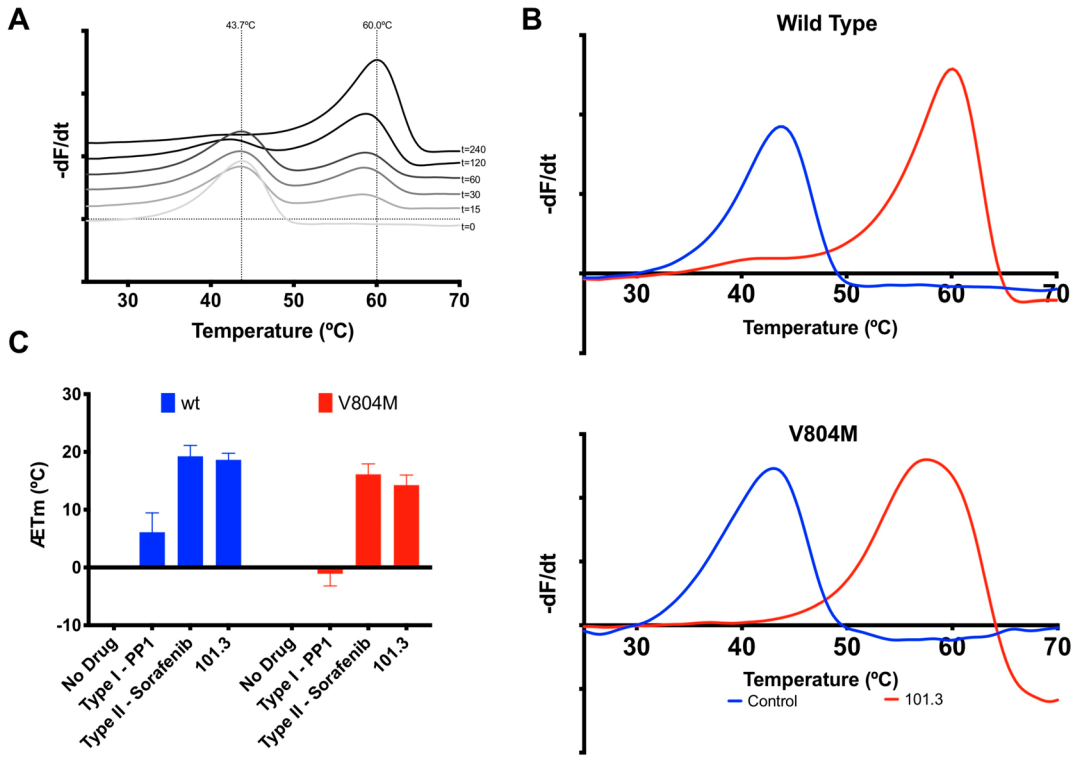

Figure 3. Thermal shift assay determination of the type 2 binding mode of NPA101.3. (A) Representative experiment of binding of NPA101.3 to the wild type RET core kinase domain monitored by the change in thermal stability. The melting temperature (T_m) is obtained from the first derivative of the change in fluorescence ($-dF/dt$) taken from the top of the peak in the derivative plot. (B) Plot of the derivative of the change in fluorescence ($-dF/dt$) for the wild type protein or V804M mutant in the presence of NPA101.3 (red) or buffer (blue) for a representative experiment. The compound binds equally well to either RET protein. (C) Tabulated average melting temperature differences (ΔT_m) from four independent experiments after the addition of NPA101.3, PP1 (a known type 1 inhibitor), or Sorafenib (a known type 2 inhibitor). The respective SD errors are shown for each drug.

10.0 nM, indicating that NPA101.3 has a similar inhibitory activity for VEGFR2 and RET (Figure 4D).

NPA101.3 inhibited RET autophosphorylation and signaling along the SHC/MAPK pathway in human cancer cell lines endogenously expressing RET oncogenic variants, including MTC cell lines, TT (RET/C634W) and MZ-CRC-1 (RET/M918T), and PTC cell line TPC-1 (CCDC6-RET); in the lung adenocarcinoma cell line Lc-2/ad (CCDC6-RET), only RET and SHC (but not MAPK) dephosphorylation was detectable (Figure S4). Virtually no effect on SHC/MAPK signaling was identified in control cell lines lacking RET oncogenes, including Nthy-ori-3.1 thyroid follicular cells, BCPAP and 8505-C, derived from thyroid cancers negative for RET oncogenes, and PC-9, A549, and CALU-1, derived from lung adenocarcinomas negative for RET oncogenes (Figure S5).

NPA101.3-Mediated Inhibition of RET-Driven Cell Proliferation. The murine pro-B cell line Ba/F3 requires IL-3 (interleukin 3) for proliferation and survival; this dependency is bypassed by active tyrosine kinases. Therefore, the Ba/F3 cell line is a standard cell culture model for determining the activity and drug-mediated inhibition of tyrosine kinases.[42] Accordingly, stable transfection of RET/C634R, RET/M918T, and CCDC6-RET oncoproteins promotes IL-3-independent growth (Figure 5). Treatment with NPA101.3 blunted RET-driven (IC_{50} values of 1.6−3.1 nM) but not IL-3-driven parental Ba/F3 cell proliferation (Figure 5), parallel to inhibition of RET phosphorylation (Figure S6).

NPA101.3 inhibited proliferation of RET mutant TT, MZ-CRC-1, TPC-1, and Lc-2/ad human cancer cells with an IC_{50} of 0.67−3.6 nM (Figure S7 and Table S4). The IC_{50} dose for all human RET-negative cells was >100.0 nM, confirming compound selectivity (Figure S8 and Table S4).

NPA101.3 Inhibits Tumorigenicity of RET-Transformed Cells. The IC_{50} dose for NPA101.3-mediated NIH3T3 RET/C634Y cell proliferation inhibition was 4.17 nM; virtually no effect was observed upon proliferation of NIH3T3 HRAS (Harvey rat sarcoma virus oncogene)/G12V cells up to 100.0 nM (Figure S9). At 10.0 nM, the compound almost completely inhibited phosphorylation of RET and SHC, and attenuated phosphorylation of MAPK, in NIH3T3 RET/C634Y cells, while virtually no effect could be detected in NIH3T3 HRAS/G12V cells up to a dose of 100.0 nM (Figure S10).

In vivo target (RET and VEGFR2) inhibition was studied by treating animals grafted with NIH3T3 RET/C634Y cells at different doses (0.3, 1, or 3 mg/kg/day p.o.) of NPA101.3 for 2 days and then performing Western blot analysis on protein extracts. As shown in Figure S11, a 3 mg/kg/day dose of NPA101.3 strongly inhibited RET autophosphorylation and signaling as well as VEGFR2 phosphorylation. Then, to determine antitumorigenic activity and to better distinguish RET- and VEGFR2-mediated effects, we tested NPA101.3 in nude mice transplanted with NIH3T3 cells transformed by either RET/C634Y or HRAS/G12V. Before tumors appeared, animals were treated daily with NPA101.3 (1.0, 3.0, or 10.0 mg/kg/day) or left untreated. NPA101.3 preferentially

https://dx.doi.org/10.1021/acs.jmedchem.9b01336
J. Med. Chem. 2020, 63, 4506−4516

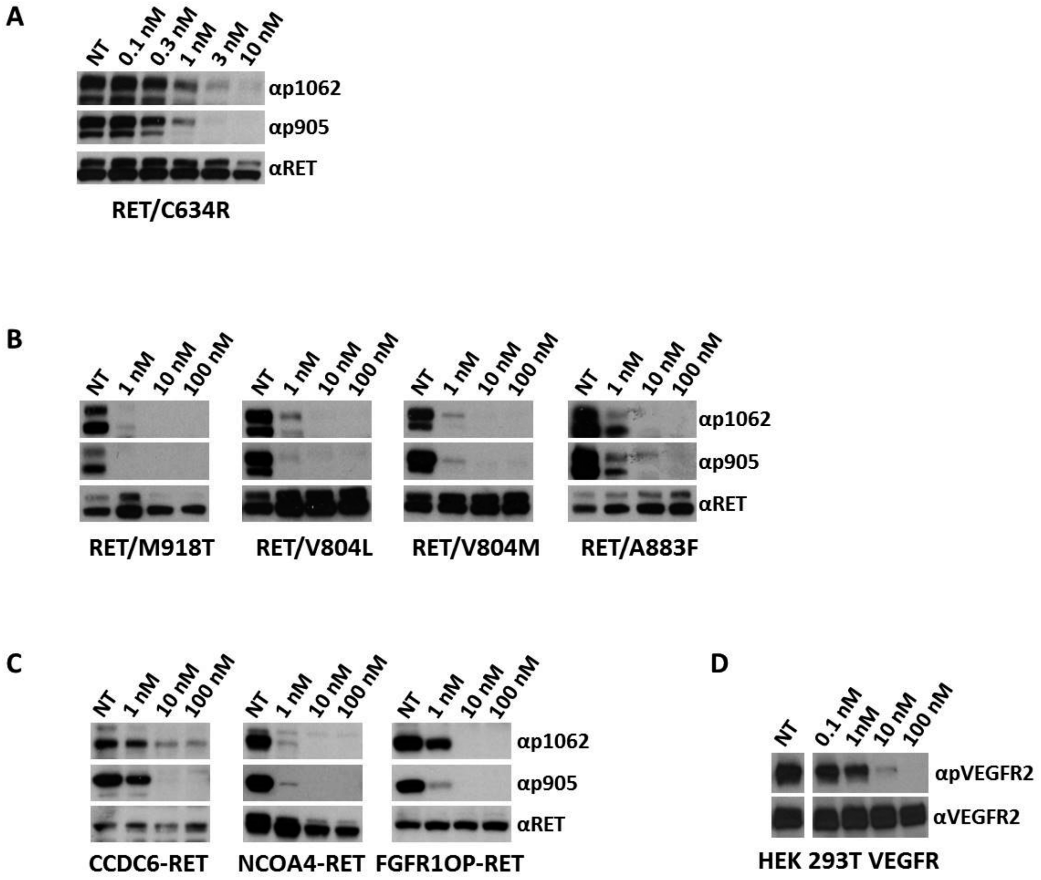

Figure 4. NPA101.3-mediated inhibition of phosphorylation and signaling of oncogenic RET mutants and VEGFR2 in intact cells. Serum-starved RAT1 cells exogenously expressing the (A and B) indicated RET point mutants or (C) NIH3T3 cells exogenously expressing the indicated RET rearranged mutants were treated for 2 h with the indicated concentrations of the compound. Total cell lysates (50 μg) were subjected to immunoblotting with anti-phospho-Y1062 (αp1062) and anti-phospho-Y905 (αp905) RET antibodies. The blots were normalized using the anti-RET (αRET) antibody. (D) HEK293 cells were transiently transfected with human VEGFR2; 36 h after transfection, cells were serum starved for 12 h. The indicated doses of the compound or vehicle (NT) were added for 2 h, and then VEGFA (100 ng/mL) stimulation was applied for 15 min. Cell lysates were immunoblotted with the anti-phospho-VEGFR2 (αpVEGFR2) antibody. The blot was normalized using the anti-VEGFR2 (αVEGFR2) antibody.

inhibited RET compared to RAS-driven tumors. While 10.0 mg of compound/kg completely prevented tumor formation induced by oncogenic RET, the treatment reduced, but did not abrogate, formation of tumors driven by RAS; moreover, at lower doses, the compound significantly reduced the rate of growth of RET-driven, but not RAS-driven, tumors (Figure 6). At 1.0 mg/kg, NPA101.3 exhibited strong RET phosphorylation and signaling inhibition in NIH3T3 RET/C634Y tumors (Figure S12); in contrast, virtually no effect on RAS signaling (MAPK phosphorylation) was detected in NIH3T3 HRAS/G12V tumors. Still, VEGFR2 inhibition was detected also in RAS-driven tumors, an effect that might explain the, albeit reduced, effect of the drug on their growth (Figure S13). Importantly, as predicted, no trace of NPA101.3 demethyl metabolites was detected after 1 or 4 h from oral dosing in mice (Figure S14). Moreover, in terms of potential toxicity, no significant change in standard blood markers of organ damage was detected upon 7 days of oral dosing (10 mg/kg/day) of NPA101.3, indicating that at this dose the compound had no general toxicity (Figure S15).

■ DISCUSSION AND CONCLUSIONS

The drug efficacy of a clinical agent is determined by target inhibition and ADMET (adsorption, distribution, metabolism, excretion, and toxicity) profiles.[32] During the IND study of the clinical TKI candidate Pz-1, we identified a major metabolic pathway initiated by phase 1 demethylation of the Pz-1 methylpyrazole substituent. Here, to generate secondary candidates with pharmacological profiles similar to that of Pz-1 but no propensity for demethylation, we replaced methylpyrazole with the metabolically resistant bioisostere (methylsulfonyl)benzene. This led to NPA101.3, a demethylation-resistant clinical candidate optimized for single-agent polypharmacology.

Molecular modeling indicated that, similar to Pz-1, NPA101.3 binds the DFG-out "inactive" conformation of RET and VEGFR2, thus functioning as a bona fide type 2 TKI.[31] This is supported experimentally by the relatively large thermal shift observed for the RET kinase−NPA101.3 complex. NPA101.3 exhibited IC_{50} values of 0.001 μM for RET and 0.003 μM for VEGFR2. It is noteworthy that, similar to Pz-1, NPA101.3 was able to bind tightly to and inhibit (IC_{50} = 0.008 μM) the RET mutant at the gatekeeper site (V804M), which is refractory to the clinical inhibitors Vandetanib and Cabozantinib.[31] NPA101.3 featured excellent selectivity for RET and VEGFR2, exhibiting affinity for only a few other kinases such as TRKs (TRKA and TRKC), CSF1R, FRK, HCK, LYN, and MKNK2. Among them, TRKA and TRKC are

https://dx.doi.org/10.1021/acs.jmedchem.9b01336
J. Med. Chem. 2020, 63, 4506−4516

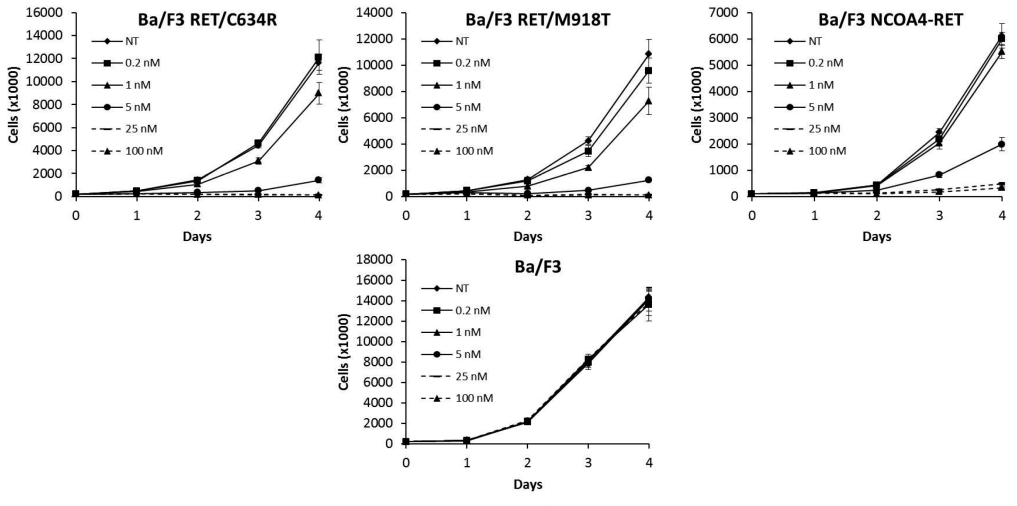

IC_{50} dose

Ba/F3 RET/C634R	1.7 nM (1.4-2.2 nM)
Ba/F3 RET/M918T	1.6 nM (1.2-2.1 nM)
Ba/F3 NCOA4-RET	3.1 nM (2.6-3.6 nM)
Ba/F3	>100 nM

Figure 5. NPA101.3-mediated inhibition of proliferation of RET-transformed Ba/F3 cells. Parental and RET/C634R-, RET M918T-, and NCOA4-RET-transfected Ba/F3 cells were incubated with vehicle (NT, not treated) or the indicated concentrations of NPA101.3 and counted at the indicated time points. Parental cells were supplemented with IL-3 (10 ng/mL). Data are the mean ± SD of a single experiment performed in triplicate. Growth inhibition IC_{50} doses of the compound for the different cell lines are reported; 95% confidence intervals are indicated in brackets.

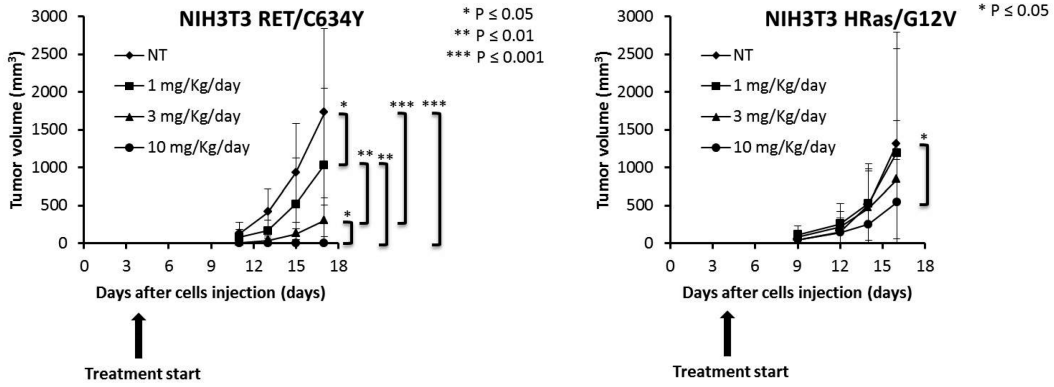

Figure 6. Effects of NPA101.3 on *in vivo* tumor growth. NIH3T3 cells transformed by RET/C634Y or HRAS/G12V were inoculated subcutaneously into nu/nu mice. After 4 days, animals were randomly assigned to receive for the indicated time periods the compound (1.0, 3.0, or 10 mg/kg/day) (24 mice; 8 mice/group for 1, 3, and 10 mg/kg doses) or vehicle (8 mice) by oral gavage. The average size of tumors is reported ± SD.

well-known driver oncogenes, which expands the potential therapeutic application of NPA101.3 beyond RET-driven cancers.[43]

In cell-based assays, NPA101.3 inhibited RET autophosphorylation and displayed a potent (IC_{50} between 0.67 and 4.17 nM) growth inhibitory effect on different types of RET (either transfected or endogenously expressing) mutant cells with no detectable effect at doses of ≤100 nM in cells negative for RET oncogenes. Finally, NPA101.3 featured efficacy already at 1 mg/kg/day in RET-driven tumors in nude mice. At higher doses (10 mg/kg/day), NPA101.3 displayed activity also against RAS-driven tumors, likely mediated by VEGFR2 inhibition. Therefore, though in a therapeutic setting toxicity may be increased by hitting multiple targets, it is feasible that the activity of the NPA101.3 against RET-driven tumors may take advantage of a synergistic combination of cell autonomous (on tumor cell growth mediated by RET inhibition) and non-cell autonomous (on blood vessel formation mediated by VEGFR2 inhibition) effects, potentiating its effect and reducing the chances of resistance development. Several TKIs with anti-RET activity are available, and some are already registered for the treatment of different types of thyroid cancers. The lesson learned from the use of TKIs in various cancer types has shown that second-line inhibitors are clinically useful when first-line treatments are hampered by toxicity and/or resistance. On the basis of potency, selectivity, and balanced RET/VEGFR2 inhibition, we posit that NPA101.3 may represent a promising, demethylation-resistant type 2 TKI for the treatment of RET-driven tumors. Studies regarding the PK profile and metabolic stability will clarify in the future how NPA101.3 is metabolized *in vivo*. This notion will be crucial to proposing NPA101.3 as a clinical candidate.

https://dx.doi.org/10.1021/acs.jmedchem.9b01336
J. Med. Chem. 2020, 63, 4506−4516

EXPERIMENTAL SECTION

General Chemistry Procedures and Synthesis of NPA101.3. All solvents were reagent grade or HPLC grade, and all starting materials were obtained from commercial sources and used without further purification. The purity of the final compounds was assessed using a Shimadzu ultra-high-throughput LC/MS system (SIL-20A, LC-20AD, LC-MS 2020, Phenomenex Onyx Monolithic C-18 Column) at variable wavelengths of 254 and 214 nm (Shimadzu PDA Detector, SPD-MN20A) and was >95%, unless otherwise noted. The HPLC mobile phase consisted of a water/acetonitrile gradient buffered with 0.1% formic acid. ^{1}H NMR spectra were recorded at 400 MHz, and ^{13}C NMR spectra were recorded at 100 MHz, both completed on a Varian 400 MHz instrument (model 4001S41ASP). All compounds were purified using silica gel (0.035−0.070 mm, 60 Å) flash chromatography, unless otherwise noted. Microwave-assisted reactions were completed in sealed vessels using a Biotage Initiator microwave synthesizer.

***In Vitro* Kinase Assays.** Kinase activity was measured by a microfluidic assay that monitors the separation of the phosphorylated product from the substrate.[31] The assay was run using a 12-sipper chip on a Caliper EZ Reader II (PerkinElmer, Waltham, MA) with separation buffer [100 mM HEPES, 10 mM EDTA, 0.015% Brij-35, and 0.1% CR-3 (PerkinElmer)]. In 96-well polypropylene plates (Greiner, Frickenhausen, Germany), compound stocks (20 mM in DMSO) were diluted into kinase buffer (50 mM HEPES, 0.075% Brij-35, 0.1% Tween 20, 2 mM DTT, 10 mM $MgCl_2$, and 0.02% NaN_3) in 12-point $^{1}/_{2}$ log dilutions (2 mM to 6.32 nM). After, 1 μL was transferred into a 384-well polypropylene assay plate (Greiner). The enzymes (RET, RET/V804M, VEGFR2, TRKA, and CSF1R) (Invitrogen, Grand Island, NY) were diluted in kinase buffer to a concentration of 2 nM, and 5 μL of the enzyme mixture was transferred to the assay plate. Kinases were preincubated with the TKI or control buffer, with gentle shaking for 60 min to allow the inhibitor to trap the DFG-out conformation; indeed, it has been reported for the type 2 (DFG-out) p38 inhibitor, BIRB-796, that an increase in incubation time increases activity.[44] A substrate mix was prepared containing ATP (Ambresco, Solon, OH) and the substrate peptide dissolved in kinase buffer, and 5 μL of the substrate mix was added to the assay plate. Running concentrations were as follows: 190 μM for ATP, 1.5 μM peptide, compound 12-point $^{1}/_{2}$ log dilutions of 0.2 mM to 0.632 nM). For a positive control, no inhibitor was added. For a negative control, no enzyme was added. The plate was run until 10−20% conversion was reached, based on the positive control wells. The following separation conditions were utilized: upstream voltage, −500 V; downstream voltage, −1900 V; chip pressure, −0.8. The percent inhibition was measured for each well comparing starting peptide to phosphorylated product peaks relative to the baseline. Dose−response curves, spanning the IC_{50} dose, were generated in GraphPad Prism 7 and fit to an exponential one-phase decay line; IC_{50} values were obtained from the half-life value of the curve. IC_{50} values were generated in triplicate.

Thermal Shift Assay. Wild type and V804M mutant RET core kinase domain proteins were expressed in SF21 cells and purified using a GST affinity tag as previously described.[45] Subsequently, both proteins were purified and phosphorylated. The affinity tag was removed using HRV 3C protease. To determine the protein thermal shifts, 3 μM recombinant proteins were incubated with DMSO (vehicle control), NPA101.3, PP1 or Sorafenib (in 100% DMSO), with a final drug concentration of 40 μM, and a final DMSO concentration of 1% (v/v). Sypro-Orange dye (Life Technologies) was added to each drug treatment, and the thermal shift was measured in a QuantStudio 12K Flex Real-Time PCR System (Applied Biosystems) over a temperature range of 25−90 °C. Subsequent analysis was performed using Protein Thermal Shift Software version 1.2 (Applied Biosystems).

Cell Cultures. NPA101.3 was dissolved in dimethyl sulfoxide (DMSO) at a concentration of 50 mM and stored at −80 °C. The final dosing solution was prepared on the day of use by dilution of the stock solution in cell growth media. RAT1 cells transformed by the various RET mutants[46] were a kind gift of M. Billaud and were cultured in DMEM with 10% fetal calf serum, 2 mM L-glutamine, and 100 units/mL penicillin-streptomycin (GIBCO). NIH3T3 cells transformed by RET/C634Y, HRAS/G12V, CCDC6-RET, NCOA4-RET, and FGFR1OP-RET were cultured in DMEM with 5% calf serum, 2 mM L-glutamine, and 100 units/mL penicillin-streptomycin (GIBCO). Parental NIH3T3 cells were grown in DMEM with 10% calf serum, 2 mM L-glutamine, and 100 units/mL penicillin-streptomycin (GIBCO). All of the RET constructs expressed in RAT1 or NIH3T3 cells encoded the short isoform of the RET protein (RET-9). Ba/F3 murine pro-B cells stably expressing NCOA4-RET, RET/C634R, and RET/M918T mutant proteins (all cloned in the long RET-51 isoform) were generated by electroporation. Parental and transformed Ba/F3 cells were cultured in RPMI supplemented with 10% fetal calf serum, 2 mM L-glutamine, and 100 units/mL penicillin-streptomycin (GIBCO), and in the case of parental cells supplemented with 10 ng/mL IL-3. CALU-1 cells, derived from a human lung adenocarcinoma, were grown in EMEM with 10% fetal calf serum, 2 mM L-glutamine, and 100 units/mL penicillin-streptomycin (GIBCO). PC-9, derived from a human lung adenocarcinoma, was grown in RPMI with 10% fetal calf serum, 2 mM L-glutamine, and 100 units/mL penicillin-streptomycin. Nthy-ori-3-1, derived from normal thyroid follicular tissue and immortalized by SV40 Large T, TPC-1, derived from a human PTC harboring CCDC6-RET,[47] BCPAP, derived from human PTC, 8505-C, derived from a human undifferentiated thyroid cancer, and A549, derived from a human lung adenocarcinoma, were cultured in DMEM with 10% fetal calf serum, 2 mM L-glutamine, and 100 units/mL penicillin-streptomycin. TT, from a human MTC harboring RET/C634W,[48] and MZ-CRC-1, from a human MTC harboring RET/M918T (a kind gift of R. F. Gagel), were cultured in RPMI with 20% fetal calf serum, 2 mM L-glutamine, and 100 units/mL penicillin-streptomycin (GIBCO). Lc-2/ad cells, derived from human lung adenocarcinoma harboring CCDC6-RET,[49] were grown in RPMI 1640/Ham's F12 (1:1) with 10% fetal calf serum, 2 mM L-glutamine, and 100 units/mL penicillin-streptomycin (GIBCO). All of the human cell lines were SNP authenticated in 2017.

Immunoblotting. Protein lysates were prepared according to standard procedures. Briefly, cells were lysed in a buffer containing 50 mM *N*-2-hydroxyethylpiperazine-*N*′-2-ethanesulfonic acid (HEPES; pH 7.5), 1% (v/v) Triton X-100, 150 mM NaCl, 5 mM EGTA, 50 mM NaF, 20 mM sodium pyrophosphate, 1 mM sodium vanadate, 2 mM phenylmethanesulfonyl fluoride (PMSF), and 1 μg/mL aprotinin. Lysates were clarified by centrifugation at 10000*g* for 15 min. Lysates containing comparable amounts of proteins, estimated by a modified Bradford assay (Bio-Rad, Munich, Germany), were subjected to direct Western blotting. Immune complexes were detected with the enhanced chemiluminescence kit (Amersham Pharmacia Biotech, Little Chalfont, U.K.). Anti-phospho-SHC (#Y317), which recognizes SHC protein when phosphorylated on Y317, was from Upstate Biotechnology Inc. (Lake Placid, NY). Anti-SHC (H-108) was from Santa Cruz Biotechnology (Santa Cruz, CA). Anti-MAPK (9101) and anti-phospho-MAPK (9102), specific for p42/44MAPK (ERK1/2) phosphorylated on Thr202/Tyr204, antibodies were from Cell Signaling Technologies (Danvers, MA). Anti-phospho-VEGFR2/KDR (2478), specific for VEGFR2/KDR phosphorylated on Tyr1175, and anti-VEGFR2/KDR (2479) were from Cell Signaling Technologies. Anti-phospho-p70S6K (9234), specific for p70S6K phosphorylated on Thr389, and anti-p70S6K (2708) were from Cell Signaling Technologies. Anti-RET is a polyclonal antibody raised against the tyrosine kinase protein fragment of human RET; anti-phospho-905 is a phospho-specific polyclonal antibody recognizing RET proteins phosphorylated at Y905, and anti-phospho-1062 is a phospho-specific polyclonal antibody recognizing RET proteins phosphorylated at Y1062.[50] Secondary antibodies coupled to horseradish peroxidase were from Santa Cruz Biotechnology.

Cell Growth Curves. Nthy-ory-3-1 (10000 per well), TPC-1 (10000 per well), MZ-CRC-1 (100000 per well), TT (200000 per well), Lc-2/ad (100000 per well), BCPAP (10000 per well), 8505-C (10000 per well), PC-9 (10000 per well), A549 (10000 per well),

https://dx.doi.org/10.1021/acs.jmedchem.9b01336
J. Med. Chem. 2020, 63, 4506−4516

CALU-1 (10000 per well), NIH3T3 RET/C634Y (10000 per well), and NIH3T3 HRAS/G12V (10000 per well) were seeded in six-well tissue culture plates. Cells were kept in 2% (TPC-1), 5% (Nthy-ori-3-1), or 10% (BCPAP, 8505-C, CALU-1, A549, PC-9, TT, MZ-CRC-1, and Lc-2/ad) fetal calf serum or in 2% (NIH3T3 RET/C634Y and HRAS/G12V) calf serum. Ba/F3 cells (200000 per well in 2 mL) were seeded in six-well tissue culture plates and kept in 10% fetal calf serum. The day after plating, different concentrations of the drug or vehicle were added to the medium and changed every 2−3 days. Cells were counted every day (Ba/F3), every 2 days (fibroblasts), or every 2−3 days (human cell lines). To compare cell growth, we performed an unpaired Student's t test using the Instat software program (Graphpad Software Inc.). All P values were two-sided, and differences were considered to be statistically significant at $P < 0.02$. IC_{50} doses were calculated through a curve fitting analysis from last day of growth curves using the PRISM software program (Graphpad Software Inc.).

Mouse Xenograft Experiments. NPA101.3 was dissolved in 80% H_2O, 19.875% Tween 20, and 0.125% xanthan gum. The formulation was stored at room temperature and vortexed prior to administration. NIH3T3 RET/C634Y (200000) or NIH3T3 HRAS/G12V (50000) cells were inoculated subcutaneously into the dorsal portion (both sides) of 6-week-old female BALB/c nu/nu mice (32 mice/cell line) (Jackson Laboratories, Bar Harbor, ME). After 4 days, before tumors had appeared, animals were randomly assigned to receive NPA101.3 (1.0, 3.0, or 10 mg/kg/day) (8 mice/group) or vehicle control (8 mice) by oral gavage. Tumor diameters were measured with caliper every 2−3 days. Tumor volumes (V) were calculated by the rotational ellipsoid formula $V = A \times B^2/2$ (A is the axial diameter, and B is the rotational diameter). No mouse showed signs of wasting or other signs of toxicity. Animals were fed *ad libitum* on an autoclaved diet and tap water and maintained at the Dipartimento di Medicina Molecolare e Biotecnologie Mediche Animal Facility. All manipulations were performed while the animals were under isoflurane gas anesthesia. Animal studies were conducted in accordance with Italian regulations for experimentation on animals and approved by the Italian Ministry of Health (Authorization 1023/2015-PR). To compare tumor growth, an unpaired Student's t test (InStat program, GraphPad Software) was used. P values were statistically significant at the $P < 0.05$ level.

■ ASSOCIATED CONTENT

Supporting Information

The Supporting Information is available free of charge at https://pubs.acs.org/doi/10.1021/acs.jmedchem.9b01336.

Molecular formula string of NPA101.3 (CSV)
Additional data (PDB)
Supplementary Methods, Tables S1−S4, and Figures S1−S14 (PDF)

Accession Codes

VEGFR2 DFG-out crystal structure, PDB entry 2OH4; amino acid sequence of RET, PDB entry 2IVU; Sorafenib in the VEGFR2 DFG-out crystal structure, PDB entry 3WZE.

■ AUTHOR INFORMATION

Corresponding Authors

Hong-yu Li − *Department of Pharmaceutical Sciences, College of Pharmacy, University of Arkansas for Medical Sciences, Little Rock, Arkansas 72205, United States; Synactix Pharmaceuticals, Inc., Tucson, Arizona 85718, United States;* orcid.org/0000-0001-9212-2010; Phone: (501) 296-1154; Email: HLi2@uams.edu

Francesca Carlomagno − *Dipartimento di Medicina Molecolare e Biotecnologie Mediche, Università di Napoli "Federico II", 80131 Napoli, Italy; Istituto di Endocrinologia ed Oncologia Sperimentale del CNR, 80131 Napoli, Italy;* orcid.org/0000-0002-1483-4677; Phone: +390815455561; Email: francesca.carlomagno@unina.it; Fax: +390817462685

Authors

Marialuisa Moccia − *Dipartimento di Medicina Molecolare e Biotecnologie Mediche, Università di Napoli "Federico II", 80131 Napoli, Italy*

Brendan Frett − *Department of Pharmaceutical Sciences, College of Pharmacy, University of Arkansas for Medical Sciences, Little Rock, Arkansas 72205, United States; Synactix Pharmaceuticals, Inc., Tucson, Arizona 85718, United States*

Lingtian Zhang − *Department of Pharmaceutical Sciences, College of Pharmacy, University of Arkansas for Medical Sciences, Little Rock, Arkansas 72205, United States*

Naga Rajiv Lakkaniga − *Department of Pharmaceutical Sciences, College of Pharmacy, University of Arkansas for Medical Sciences, Little Rock, Arkansas 72205, United States;* orcid.org/0000-0001-8370-2224

David C. Briggs − *Signalling and Structural Biology Laboratory, The Francis Crick Institute, London NW1 1AT, U.K.*

Rakhee Chauhan − *Signalling and Structural Biology Laboratory, The Francis Crick Institute, London NW1 1AT, U.K.*

Annalisa Brescia − *Dipartimento di Medicina Molecolare e Biotecnologie Mediche, Università di Napoli "Federico II", 80131 Napoli, Italy*

Giorgia Federico − *Dipartimento di Medicina Molecolare e Biotecnologie Mediche, Università di Napoli "Federico II", 80131 Napoli, Italy*

Wei Yan − *Department of Pharmaceutical Sciences, College of Pharmacy, University of Arkansas for Medical Sciences, Little Rock, Arkansas 72205, United States*

Massimo Santoro − *Dipartimento di Medicina Molecolare e Biotecnologie Mediche, Università di Napoli "Federico II", 80131 Napoli, Italy*

Neil Q. McDonald − *Signalling and Structural Biology Laboratory, The Francis Crick Institute, London NW1 1AT, U.K.; Institute of Structural and Molecular Biology, Department of Biological Sciences, Birkbeck College, London WC1E 7HX, U.K.*

Complete contact information is available at: https://pubs.acs.org/10.1021/acs.jmedchem.9b01336

Author Contributions

M.M. and B.F. contributed equally to this work. M.M., A.B., and G.F. performed the cell-based and animal-based experiments. B.F., L.Z., W.Y., and N.R.L. performed the synthesis, the modeling studies, and the *in vitro* kinase assays. D.C.B. and R.C. performed the thermal shift assay. M.S. and N.Q.M. participated in experiment planning and data analysis. H.L. and F.C. participated in experiment planning and data analysis and wrote the manuscript.

Funding

This study was supported by NIH Grant 1R01CA197178-01A1R (to H.L.). In addition, H.L. was supported by NIH Grant 1R01CA194094-010 and University of Arkansas for Medical Sciences (UAMS) start-up funding. F.C. was supported by the Associazione Italiana per la Ricerca sul Cancro (AIRC). N.Q.M. was supported by the Francis Crick Institute, which receives its core funding from Cancer Research UK (FC001115), the UK Medical Research Council (FC001115), and the Wellcome Trust (FC001115). R.C.

was supported by a grant to NQM from the Association for Multiple Endocrine Neoplasia Disorders MTC Research Fund. This work was also supported by an Institutional Development Award (IDeA) from the National Institute of General Medical Sciences of the National Institutes of Health under Grant P20 GM109005, by the UAMS Seeds of Science cancer research grant, by a grant from the American Thyroid Association (ATA/Thyca), and by the POR Campania FESR 2014−2020 "SATIN" grant.

Notes

The authors declare the following competing financial interest(s): B.F. and H.L. have ownership interest in Synactix Pharmaceuticals, Inc. F.C., B.F., M.S., and H.L. are inventors of patent WO/2015/187818. D.C.B., R.C., and N.Q.M. declare no potential conflicts of interest.

■ ACKNOWLEDGMENTS

MZ-CRC-1 cells and RAT1 cells expressing RET mutants were kindly donated by R. F. Gagel (M. D. Anderson Cancer Center) and by M. Billaud (Institut Albert Bonniot, Grenoble, France), respectively.

■ ABBREVIATIONS USED

A, alanine; ADMET, adsorption, distribution, metabolism, excretion, and toxicity; C, cysteine; CCDC6, coiled-coil domain containing 6; CSF1R, colony stimulating factor 1 receptor; D, aspartic acid; EGFR, epidermal growth factor receptor; F, phenylalanine; FGFR1OP, fibroblast growth factor receptor 1 oncogene partner; FRK, fyn-related Src family tyrosine kinase; G, glycine; GDNF, glial cell line-derived neurotrophic factor; HCK, HCK proto-oncogene, Src family tyrosine kinase; hERG, potassium voltage-gated channel subfamily H member 2; HRAS, Harvey rat sarcoma virus oncogene; IC_{50}, inhibitory concentration 50; IL-3, interleukin 3; IND, investigative new drug; K, lysine; L, leucine; LYN, LYN proto-oncogene, Src family tyrosine kinase; M, methionine; MAPK, mitogen-activated protein kinase; MEN2, multiple endocrine neoplasia type 2; MKNK2, MAPK-interacting serine/threonine kinase 2; MTC, medullary thyroid carcinoma; NCOA4, nuclear coactivator 4; PDB, Protein Data Bank; PK, pharmacokinetics; PTC, papillary thyroid carcinoma; R, arginine; RET, rearranged during transfection; RTK, receptor tyrosine kinase; SAR, structure−activity relationship; SHC, SHC adaptor protein 1; T, threonine; TK, tyrosine kinase; TKI, tyrosine kinase inhibitor; TRKA, neurotrophic receptor tyrosine kinase 1; TRKC, neurotrophic receptor tyrosine kinase 3; V, valine; VEGFR2, vascular endothelial growth factor receptor 2; W, tryptophan; Y, tyrosine

■ REFERENCES

(1) Mulligan, L. M. RET Revisited: Expanding the Oncogenic Portfolio. *Nat. Rev. Cancer* **2014**, *14*, 173−186.

(2) Agrawal, N.; Cancer Genome Atlas Research Network; et al. Integrated Genomic Characterization of Papillary Thyroid Carcinoma. *Cell* **2014**, *159*, 676−690.

(3) Grubbs, E. G.; Ng, P. K.; Bui, J.; Busaidy, N. L.; Chen, K.; Lee, J. E.; Lu, X.; Lu, H.; Meric-Bernstam, F.; Mills, G. B.; Palmer, G.; Perrier, N. D.; Scott, K. L.; Shaw, K. R.; Waguespack, S. G.; Williams, M. D.; Yelensky, R.; Cote, G. J. RET Fusion as a Novel Driver of Medullary Thyroid Carcinoma. *J. Clin. Endocrinol. Metab.* **2015**, *100*, 788−793.

(4) Kohno, T.; Ichikawa, H.; Totoki, Y.; Yasuda, K.; Hiramoto, M.; Nammo, T.; Sakamoto, H.; Tsuta, K.; Furuta, K.; Shimada, Y.; Iwakawa, R.; Ogiwara, H.; Oike, T.; Enari, M.; Schetter, A. J.; Okayama, H.; Haugen, A.; Skaug, V.; Chiku, S.; Yamanaka, I.; Arai, Y.; Watanabe, S.; Sekine, I.; Ogawa, S.; Harris, C. C.; Tsuda, H.; Yoshida, T.; Yokota, J.; Shibata, T. KIF5B-RET Fusions in Lung Adenocarcinoma. *Nat. Med.* **2012**, *18*, 375−377.

(5) Takeuchi, K.; Soda, M.; Togashi, Y.; Suzuki, R.; Sakata, S.; Hatano, S.; Asaka, R.; Hamanaka, W.; Ninomiya, H.; Uehara, H.; Lim Choi, Y.; Satoh, Y.; Okumura, S.; Nakagawa, K.; Mano, H.; Ishikawa, Y. RET, ROS1 and ALK Fusions in Lung Cancer. *Nat. Med.* **2012**, *18*, 378−381.

(6) Lipson, D.; Capelletti, M.; Yelensky, R.; Otto, G.; Parker, A.; Jarosz, M.; Curran, J. A.; Balasubramanian, S.; Bloom, T.; Brennan, K. W.; Donahue, A.; Downing, S. R.; Frampton, G. M.; Garcia, L.; Juhn, F.; Mitchell, K. C.; White, E.; White, J.; Zwirko, Z.; Peretz, T.; Nechushtan, H.; Soussan-Gutman, L.; Kim, J.; Sasaki, H.; Kim, H. R.; Park, S. I.; Ercan, D.; Sheehan, C. E.; Ross, J. S.; Cronin, M. T.; Jänne, P. A.; Stephens, P. J. Identification of New ALK and RET Gene Fusions from Colorectal and Lung Cancer Biopsies. *Nat. Med.* **2012**, *18*, 382−384.

(7) Ballerini, P.; Struski, S.; Cresson, C.; Prade, N.; Toujani, S.; Deswarte, C.; Dobbelstein, S.; Petit, A.; Lapillonne, H.; Gautier, E. F.; Demur, C.; Lippert, E.; Pages, P.; Mansat-De Mas, V.; Donadieu, J.; Huguet, F.; Dastugue, N.; Broccardo, C.; Perot, C.; Delabesse, E. RET Fusion Genes are Associated with Chronic Myelomonocytic Leukemia and Enhance Monocytic Differentiation. *Leukemia* **2012**, *26*, 2384−2389.

(8) Bossi, D.; Carlomagno, F.; Pallavicini, I.; Pruneri, G.; Trubia, M.; Raviele, P. R.; Marinelli, A.; Anaganti, S.; Cox, M. C.; Viale, G.; Santoro, M.; Di Fiore, P. P.; Minucci, S. Functional Characterization of a Novel FGFR1OP-RET Rearrangement in Hematopoietic Malignancies. *Mol. Oncol.* **2014**, *8*, 221−231.

(9) Wiesner, T.; He, J.; Yelensky, R.; Esteve-Puig, R.; Botton, T.; Yeh, I.; Lipson, D.; Otto, G.; Brennan, K.; Murali, R.; Garrido, M.; Miller, V. A.; Ross, J. S.; Berger, M. F.; Sparatta, A.; Palmedo, G.; Cerroni, L.; Busam, K. J.; Kutzner, H.; Cronin, M. T.; Stephens, P. J.; Bastian, B. C. Kinase Fusions are Frequent in Spitz Tumours and Spitzoid Melanomas. *Nat. Commun.* **2014**, *5*, 3116.

(10) Le Rolle, A. F.; Klempner, S. J.; Garrett, C. R.; Seery, T.; Sanford, E. M.; Balasubramanian, S.; Ross, J. S.; Stephens, P. J.; Miller, V. A.; Ali, S. M.; Chiu, V. K. Identification and Characterization of RET Fusions in Advanced Colorectal Cancer. *Oncotarget* **2015**, *6*, 28929−28937.

(11) Hechtman, J. F.; Zehir, A.; Yaeger, R. D.; Wang, L.; Middha, S.; Zheng, T.; Hyman, D.; Solit, D.; Arcila, M. E.; Borsu, L.; Shia, J.; Vakiani, E.; Saltz, L.; Ladanyi, M. Identification of Targetable Kinase Alterations in Patients with Colorectal Carcinoma that are Preferentially Associated with Wild Type RAS/RAF. *Mol. Cancer Res.* **2016**, *14*, 296−301.

(12) Paratala, B. S.; Chung, J. H.; Williams, C. B.; Yilmazel, B.; Petrosky, W.; Williams, K.; Schrock, A. B.; Gay, L. M.; Lee, E.; Dolfi, S. C.; Pham, K.; Lin, S.; Yao, M.; Kulkarni, A.; DiClemente, F.; Liu, C.; Rodriguez-Rodriguez, L.; Ganesan, S.; Ross, J. S.; Ali, S. M.; Leyland-Jones, B.; Hirshfield, K. M. RET Rearrangements are Actionable Alterations in Breast Cancer. *Nat. Commun.* **2018**, *9*, 4821.

(13) Wang, K.; Russell, J. S.; McDermott, J. D.; Elvin, J. A.; Khaira, D.; Johnson, A.; Jennings, T. A.; Ali, S. M.; Murray, M.; Marshall, C.; Oldham, D. S.; Washburn, D.; Wong, S. J.; Chmielecki, J.; Yelensky, R.; Lipson, D.; Miller, V. A.; Stephens, P. J.; Serracino, H. S.; Ross, J. S.; Bowles, D. W. Profiling of 149 Salivary Duct Carcinomas, Carcinoma Ex Pleomorphic Adenomas, and Adenocarcinomas, Not Otherwise Specified Reveals Actionable Genomic Alterations. *Clin. Cancer Res.* **2016**, *22*, 6061−6068.

(14) Klempner, S. J.; Bazhenova, L. A.; Braiteh, F. S.; Nikolinakos, P. G.; Gowen, K.; Cervantes, C. M.; Chmielecki, J.; Greenbowe, J. R.; Ross, J. S.; Stephens, P. J.; Miller, V. A.; Ali, S. M.; Ou, S. H. Emergence of RET Rearrangement Co-Existing with Activated EGFR Mutation in EGFR-Mutated NSCLC Patients who had Progressed on

https://dx.doi.org/10.1021/acs.jmedchem.9b01336
J. Med. Chem. 2020, 63, 4506−4516

First- or Second-Generation EGFR TKI. *Lung Cancer* **2015**, *89*, 357−359.
(15) Wells, S. A., Jr.; Pacini, F.; Robinson, B. G.; Santoro, M. Multiple Endocrine Neoplasia Type 2 and Familial Medullary Thyroid Carcinoma: an Update. *J. Clin. Endocrinol. Metab.* **2013**, *98*, 3149−3164.
(16) Morandi, A.; Plaza-Menacho, I.; Isacke, C. M. RET in Breast Cancer: Functional and Therapeutic Implications. *Trends Mol. Med.* **2011**, *17*, 149−157.
(17) Nguyen, M.; Miyakawa, S.; Kato, J.; Mori, T.; Arai, T.; Armanini, M.; Gelmon, K.; Yerushalmi, R.; Leung, S.; Gao, D.; Landes, G.; Haak-Frendscho, M.; Elias, K.; Simmons, A. D. Preclinical Efficacy and Safety Assessment of an Antibody-Drug Conjugate Targeting the c-RET Proto-Oncogene for Breast Carcinoma. *Clin. Cancer Res.* **2015**, *21*, 5552−5562.
(18) Gil, Z.; Cavel, O.; Kelly, K.; Brader, P.; Rein, A.; Gao, S. P.; Carlson, D. L.; Shah, J. P.; Fong, Y.; Wong, R. J. Paracrine Regulation of Pancreatic Cancer cell Invasion by Peripheral Nerves. *J. Natl. Cancer Inst.* **2010**, *102*, 107−118.
(19) He, S.; Chen, C. H.; Chernichenko, N.; He, S.; Bakst, R. L.; Barajas, F.; Deborde, S.; Allen, P. J.; Vakiani, E.; Yu, Z.; Wong, R. J. GFRα1 Released by Nerves Enhances Cancer Cell Perineural Invasion through GDNF-RET Signaling. *Proc. Natl. Acad. Sci. U. S. A.* **2014**, *111*, E2008−E2017.
(20) De Falco, V.; Carlomagno, F.; Li, H. Y.; Santoro, M. The Molecular Basis for RET Tyrosine-kinase Inhibitors in Thyroid Cancer. *Best Pract. Res. Clin. Endocrinol. Metab.* **2017**, *31*, 307−318.
(21) Drilon, A.; Hu, Z. I.; Lai, G. G. Y.; Tan, D. S. W. Targeting RET-Driven Cancers: Lessons from Evolving Preclinical and Clinical Landscapes. *Nat. Rev. Clin. Oncol.* **2018**, *15*, 151−167.
(22) Commander, H.; Whiteside, G.; Perry, C. Vandetanib: First Global Approval. *Drugs* **2011**, *71*, 1355−1365.
(23) Grüllich, C. Cabozantinib: a MET, RET, and VEGFR2 Tyrosine Kinase Inhibitor. *Recent Results Cancer Res.* **2014**, *201*, 207−214.
(24) Wells, S. A., Jr.; Robinson, B. G.; Gagel, R. F.; Dralle, H.; Fagin, J. A.; Santoro, M.; Baudin, E.; Elisei, R.; Jarzab, B.; Vasselli, J. R.; Read, J.; Langmuir, P.; Ryan, A. J.; Schlumberger, M. J. Vandetanib in Patients with Locally Advanced or Metastatic Medullary Thyroid Cancer: a Randomized, Double-Blind Phase III trial. *J. Clin. Oncol.* **2012**, *30*, 134−141.
(25) Elisei, R.; Schlumberger, M. J.; Müller, S. P.; Schöffski, P.; Brose, M. S.; Shah, M. H.; Licitra, L.; Jarzab, B.; Medvedev, V.; Kreissl, M. C.; Niederle, B.; Cohen, E. E.; Wirth, L. J.; Ali, H.; Hessel, C.; Yaron, Y.; Ball, D.; Nelkin, B.; Sherman, S. I. Cabozantinib in Progressive Medullary Thyroid Cancer. *J. Clin. Oncol.* **2013**, *31*, 3639−3646.
(26) Schlumberger, M.; Tahara, M.; Wirth, L. J.; Robinson, B.; Brose, M. S.; Elisei, R.; Habra, M. A.; Newbold, K.; Shah, M. H.; Hoff, A. O.; Gianoukakis, A. G.; Kiyota, N.; Taylor, M. H.; Kim, S. B.; Krzyzanowska, M. K.; Dutcus, C. E.; de las Heras, B.; Zhu, J.; Sherman, S. I. Lenvatinib Versus Placebo in Radioiodine-Refractory Thyroid Cancer. *N. Engl. J. Med.* **2015**, *372*, 621−630.
(27) White, P. T.; Cohen, M. S. The Discovery and Development of Sorafenib for the Treatment of Thyroid Cancer. *Expert Opin. Drug Discovery* **2015**, *10*, 427−439.
(28) Subbiah, V.; Gainor, J. F.; Rahal, R.; Brubaker, J. D.; Kim, J. L.; Maynard, M.; Hu, W.; Cao, Q.; Sheets, M. P.; Wilson, D.; Wilson, K. J.; DiPietro, L.; Fleming, P.; Palmer, M.; Hu, M. I.; Wirth, L.; Brose, M. S.; Ou, S. I.; Taylor, M.; Garralda, E.; Miller, S.; Wolf, B.; Lengauer, C.; Guzi, T.; Evans, E. K. Precision Targeted Therapy with BLU-667 for RET-Driven Cancers. *Cancer Discovery* **2018**, *8*, 836−849.
(29) Subbiah, V.; Velcheti, V.; Tuch, B. B.; Ebata, K.; Busaidy, N. L.; Cabanillas, M. E.; Wirth, L. J.; Stock, S.; Smith, S.; Lauriault, V.; Corsi-Travali, S.; Henry, D.; Burkard, M.; Hamor, R.; Bouhana, K.; Winski, S.; Wallace, R. D.; Hartley, D.; Rhodes, S.; Reddy, M.; Brandhuber, B. J.; Andrews, S.; Rothenberg, S. M.; Drilon, A. Selective RET Kinase Inhibition for Patients with RET-Altered Cancers. *Ann. Oncol.* **2018**, *29*, 1869−1876.
(30) Drilon, A.; Fu, S.; Patel, M. R.; Fakih, M.; Wang, D.; Olszanski, A. J.; Morgensztern, D.; Liu, S. V.; Cho, B. C.; Bazhenova, L.; Rodriguez, C. P.; Doebele, R. C.; Wozniak, A.; Reckamp, K. L.; Seery, T.; Nikolinakos, P.; Hu, Z.; Oliver, J. W.; Trone, D.; McArthur, K.; Patel, R.; Multani, P. S.; Ahn, M. J. A Phase I/Ib Trial of the VEGFR-Sparing Multikinase RET Inhibitor RXDX-105. *Cancer Discovery* **2019**, *9*, 384−395.
(31) Frett, B.; Carlomagno, F.; Moccia, M. L.; Brescia, A.; Federico, G.; De Falco, V.; Admire, B.; Chen, Z.; Qi, W.; Santoro, M.; Li, H. Y. Fragment-Based Discovery of a Dual pan-RET/VEGFR2 Kinase Inhibitor Optimized for Single-Agent Polypharmacology. *Angew. Chem., Int. Ed.* **2015**, *54*, 8717−8721.
(32) Yamazaki, H. Drug-Metabolizing Enzyme Systems I. In *Comprehensive Medicinal Chemistry III*; Chackalamannil, S., Rotella, D., Ward, S., Eds.; Elsevier: Amsterdam, 2017; pp 45−50.
(33) Zhang, J.; Yang, P. L.; Gray, N. S. Targeting Cancer with Small Molecule Kinase Inhibitors. *Nat. Rev. Cancer* **2009**, *9*, 28−39.
(34) Carlomagno, F.; Guida, T.; Anaganti, S.; Vecchio, G.; Fusco, A.; Ryan, A. J.; Billaud, M.; Santoro, M. Disease Associated Mutations at Valine 804 in the RET Receptor Tyrosine Kinase Confer Resistance to Selective Kinase Inhibitors. *Oncogene* **2004**, *23*, 6056−6063.
(35) Mologni, L.; Redaelli, S.; Morandi, A.; Plaza-Menacho, I.; Gambacorti-Passerini, C. Ponatinib is a Potent Inhibitor of Wild-Type and Drug-Resistant Gatekeeper Mutant RET Kinase. *Mol. Cell. Endocrinol.* **2013**, *377*, 1−6.
(36) Plenker, D.; Riedel, M.; Brägelmann, J.; Dammert, M. A.; Chauhan, R.; Knowles, P. P.; Lorenz, C.; Keul, M.; Bührmann, M.; Pagel, O.; Tischler, V.; Scheel, A. H.; Schütte, D.; Song, Y.; Stark, J.; Mrugalla, F.; Alber, Y.; Richters, A.; Engel, J.; Leenders, F.; Heuckmann, J. M.; Wolf, J.; Diebold, J.; Pall, G.; Peifer, M.; Aerts, M.; Gevaert, K.; Zahedi, R. P.; Buettner, R.; Shokat, K. M.; McDonald, N. Q.; Kast, S. M.; Gautschi, O.; Thomas, R. K.; Sos, M. L. Drugging the Catalytically Inactive State of RET kinase in RET-Rearranged Tumors. *Sci. Transl. Med.* **2017**, *9*, eaah6144.
(37) Vedadi, M.; Niesen, F. H.; Allali-Hassani, A.; Fedorov, O. Y.; Finerty, P. J., Jr.; Wasney, G. A.; Yeung, R.; Arrowsmith, C.; Ball, L. J.; Berglund, H.; Hui, R.; Marsden, B. D.; Nordlund, P.; Sundstrom, M.; Weigelt, J.; Edwards, A. M. Chemical Screening Methods to Identify Ligands that Promote Protein Stability, Protein Crystallization, and Structure Determination. *Proc. Natl. Acad. Sci. U. S. A.* **2006**, *103*, 15835−15840.
(38) Nakaoku, T.; Kohno, T.; Araki, M.; Niho, S.; Chauhan, R.; Knowles, P. P.; Tsuchihara, K.; Matsumoto, S.; Shimada, Y.; Mimaki, S.; Ishii, G.; Ichikawa, H.; Nagatoishi, S.; Tsumoto, K.; Okuno, Y.; Yoh, K.; McDonald, N. Q.; Goto, K. A Secondary RET Mutation in the Activation Loop Conferring Resistance to Vandetanib. *Nat. Commun.* **2018**, *9*, 625.
(39) Bullock, A. N.; Debreczeni, J. E.; Fedorov, O. Y.; Nelson, A.; Marsden, B. D.; Knapp, S. Structural Basis of Inhibitor Specificity of the Human Protooncogene Proviral Insertion Site in Moloney Murine Leukemia Virus (PIM-1) Kinase. *J. Med. Chem.* **2005**, *48*, 7604−7614.
(40) Kufareva, I.; Abagyan, R. Type-II Kinase Inhibitor Docking, Screening, and Profiling Using Modified Structures of Active Kinase States. *J. Med. Chem.* **2008**, *51*, 7921−7932.
(41) Plaza-Menacho, I.; Barnouin, K.; Goodman, K.; Martínez-Torres, R. J.; Borg, A.; Murray-Rust, J.; Mouilleron, S.; Knowles, P.; McDonald, N. Q. Oncogenic RET Kinase Domain Mutations Perturb the Autophosphorylation Trajectory by Enhancing Substrate Presentation in Trans. *Mol. Cell* **2014**, *53*, 738−751.
(42) Kitayama, H.; Kanakura, Y.; Furitsu, T.; Tsujimura, T.; Oritani, K.; Ikeda, H.; Sugahara, H.; Mitsui, H.; Kanayama, Y.; Kitamura, Y. Constitutively Activating Mutations of C-Kit Receptor Tyrosine Kinase Confer Factor-Independent Growth and Tumorigenicity of Factor-Dependent Hematopoietic Cell Lines. *Blood* **1995**, *85*, 790−798.

https://dx.doi.org/10.1021/acs.jmedchem.9b01336
J. Med. Chem. 2020, 63, 4506−4516

(43) Yan, W.; Lakkaniga, N. R.; Carlomagno, F.; Santoro, M.; McDonald, N. Q.; Lv, F.; Gunaganti, N.; Frett, B.; Li, H. Y. Insights into Current Tropomyosin Receptor Kinase (TRK) Inhibitors: Development and Clinical Application. *J. Med. Chem.* **2019**, *62*, 1731−1760.
(44) Pargellis, C.; Tong, L.; Churchill, L.; Cirillo, P. F.; Gilmore, T.; Graham, A. G.; Grob, P. M.; Hickey, E. R.; Moss, N.; Pav, S.; Regan, J. Inhibition of p38 MAP Kinase by Utilizing a Novel Allosteric Binding Site. *Nat. Struct. Biol.* **2002**, *9*, 268−272.
(45) Knowles, P. P.; Murray-Rust, J.; Kjaer, S.; Scott, R. P.; Hanrahan, S.; Santoro, M.; Ibáñez, C. F.; McDonald, N. Q. Structure and Chemical Inhibition of the RET Tyrosine Kinase Domain. *J. Biol. Chem.* **2006**, *281*, 33577−33587.
(46) Pasini, A.; Geneste, O.; Legrand, P.; Schlumberger, M.; Rossel, M.; Fournier, L.; Rudkin, B. B.; Schuffenecker, I.; Lenoir, G. M.; Billaud, M. Oncogenic Activation of RET by Two Distinct FMTC Mutations Affecting the Tyrosine Kinase Domain. *Oncogene* **1997**, *15*, 393−402.
(47) Ishizaka, Y.; Ushijima, T.; Sugimura, T.; Nagao, M. cDNA Cloning and Characterization of Ret Activated in a Human Papillary Thyroid Carcinoma Cell Line. *Biochem. Biophys. Res. Commun.* **1990**, *168*, 402−408.
(48) Carlomagno, F.; Salvatore, D.; Santoro, M.; de Franciscis, V.; Quadro, L.; Panariello, L.; Colantuoni, V.; Fusco, A. Point Mutation of the RET Proto-Oncogene in the TT Human Medullary Thyroid Carcinoma Cell Line. *Biochem. Biophys. Res. Commun.* **1995**, *207*, 1022−1028.
(49) Suzuki, M.; Makinoshima, H.; Matsumoto, S.; Suzuki, A.; Mimaki, S.; Matsushima, K.; Yoh, K.; Goto, K.; Suzuki, Y.; Ishii, G.; Ochiai, A.; Tsuta, K.; Shibata, T.; Kohno, T.; Esumi, H.; Tsuchihara, K. Identification of a Lung Adenocarcinoma Cell Line with CCDC6-RET Fusion Gene and the Effect of RET Inhibitors in Vitro and in Vivo. *Cancer Sci.* **2013**, *104*, 896−903.
(50) Carlomagno, F.; Vitagliano, D.; Guida, T.; Basolo, F.; Castellone, M. D.; Melillo, R. M.; Fusco, A.; Santoro, M. Efficient Inhibition of RET/Papillary Thyroid Carcinoma Oncogenic Kinases by 4-amino-5-(4-chloro-phenyl)-7-(t-butyl)pyrazolo[3,4-d]-pyrimidine (PP2). *J. Clin. Endocrinol. Metab.* **2003**, *88*, 1897−1902.

https://dx.doi.org/10.1021/acs.jmedchem.9b01336
J. Med. Chem. 2020, 63, 4506−4516